Journal of Environmental Management 373 (2025) 123957

Contents lists available at ScienceDirect

Journal of Environmental Management

journal homepage: www.elsevier.com/locate/jenvman

Research article

A chemometric approach to the interaction of hydrogen peroxide and thermally activated persulfate in the removal of aromatic compounds

Antonio Faggiano [a], Ana B. Martínez-Piernas [b], Maria Ricciardi [a], Oriana Motta [c], Antonino Fiorentino [d,*], Antonio Proto [a]

[a] Department of Chemistry and Biology "Adolfo Zambelli", University of Salerno, via Giovanni Paolo II 132, 84084, Fisciano, SA, Italy
[b] Department of Analytical Chemistry, Faculty of Sciences, University of Malaga, 29071, Malaga, Spain
[c] Department of Medicine Surgery and Dentistry "Scuola Medica Salernitana", University of Salerno, via S. Allende 1, 84081, Baronissi, SA, Italy
[d] Department of Chemistry, University of Milan, Via Golgi 19, 20133, Milan, Italy

ARTICLE INFO

Keywords:
Advanced oxidation processes
Dual oxidant system
Phenol degradation
Kinetic modelling
Wastewater treatment

ABSTRACT

This study evaluates the combined use of H_2O_2 and thermally activated $S_2O_8^{2-}$ (T-PDS) for the degradation of phenolic compounds (PhOH) in wastewater, aiming to limit or eliminate sludge production. Phenolic compounds are common in industrial effluents, and their effective removal is crucial for reducing environmental impact. The study employs Response Surface Methodology (RSM) and Principal Component Analysis (PCA) to optimise critical variables such as temperature, pH, and oxidant concentrations. Optimal conditions were determined to be a temperature of 70 °C, pH 5, and a $H_2O_2/S_2O_8^{2-}$ molar ratio of 1:6. Under these conditions, the system achieved an 89% PhOH degradation efficiency, reducing the concentration from 10 to 1.2 mg L^{-1} after 120 min of treatment. The kinetic analysis revealed a rapid initial reduction in PhOH concentration by 38% (from 10 to 6.2 mg L^{-1}) within the first 15 min, followed by a slower degradation phase. This suggests a complex reaction mechanism, likely influenced by oxidant consumption and intermediate formation. The model demonstrated high precision, with R^2 values of 0.99 for PhOH and $S_2O_8^{2-}$and slightly lower for H_2O_2 ($R^2 = 0.98$). A brief cost analysis estimated the treatment cost at €6.86 per cubic meter of wastewater, showing the economic viability of the process. Additionally, eliminating sludge formation reduces operational costs related to sludge management and disposal, making the H_2O_2/T-PDS system a promising solution for large-scale industrial applications in sustainable wastewater treatment.

1. Introduction

Removing persistent organic pollutants such as phenolic compounds, pharmaceuticals, and dyes from wastewater is one of the most pressing environmental challenges. Advanced Oxidation Processes (AOPs) are gaining attention for their effectiveness in breaking down persistent organic pollutants such as phenolic compounds, pharmaceuticals, and dyes (Faggiano et al., 2023a; Akbari et al., 2021; Fiorentino et al., 2022; Nidheesh et al., 2018). Phenolic compounds, widely used in industries such as plastics, resins, pharmaceuticals, and pesticides, are common persistent organic pollutants in wastewater. Their toxicity, carcinogenicity, and mutagenicity pose significant risks to human health and ecosystems, with phenol concentrations in industrial effluents ranging from 0.1 to 300 mg L^{-1}, often exceeding regulatory limits set by the US EPA and the European Commission (Samarghandi et al., 2021a; Almasi et al., 2021; Bazrafshan et al., 2023a). Exposure to phenolics can cause neurological, renal, and hepatic damage, while derivatives like pentachlorophenol and bisphenol A exhibit endocrine-disrupting effects (Dargahi et al., 2023; Samarghandi et al., 2021b; Shokoohi et al., 2018). Various methods for phenol removal from wastewater have been explored, including biological treatments like activated sludge and sequencing batch reactors, physical methods such as adsorption, and chemical methods including AOPs (Dargahi et al., 2023; Shokoohi et al., 2018). Among these, AOPs have gained significant attention due to their ability to mineralize complex organic molecules without generating sludge (Almasi et al., 2021; Bazrafshan et al., 2023a). AOPs stand out for

Abbreviations: AOPs, advanced oxidation processes; CCD, central-composite design; COD, chemical oxygen demand; HP, hydrogen peroxide; PCA, principal component analysis; PDS, peroxydisulfate; ROSs, reactive oxidative species; RSM, response surface methodology.

* Corresponding author.
E-mail address: antonino.fiorentino@unimi.it (A. Fiorentino).

https://doi.org/10.1016/j.jenvman.2024.123957
Received 18 September 2024; Received in revised form 4 December 2024; Accepted 27 December 2024
Available online 30 December 2024

their ability to mineralize pollutants without generating sludge, though limitations such as sensitivity to conditions and high energy input remain (Samarghandi et al., 2021a, 2021b). These processes leverage Reactive Oxidative Species (ROSs) like hydroxyl radicals ($^{\bullet}OH$) with an oxidation potential of 1.8–2.7 V and sulphate radicals ($SO_4^{\bullet-}$) with a potential of 2.5–3.1 V. AOPs work by activating various oxidants, including hydrogen peroxide (H_2O_2), persulfate ($S_2O_8^{2-}$) and ozone (O_3) (Faggiano et al., 2023b; Iakovides et al., 2021; Karim et al., 2021). AOPs have a wide range of applications, from treating target compounds and real wastewater to the disinfection of effluents (Fiorentino et al., 2021; Faggiano et al., 2022; Attar et al., 2023; Brillas and Garcia-Segura, 2020). Peroxydisulfate (PDS, $S_2O_8^{2-}$) exhibits a high redox potential and contains a single O–O bonds. However, it has a high bond energy (140 kJ/mol) and does not readily react directly with organic matter. It is typically necessary to activate the single O–O bond to produce $SO_4^{\bullet-}$ or $^{\bullet}OH$ indirectly (Karim et al., 2021; Wang and Wang, 2022; Macías-Vargas et al., 2021) as shown by Eq. (1) and Eq. (2).

$$S_2O_8^{2-} \rightarrow 2SO_4^{\cdot-} \quad \text{Eq. 1}$$

$$SO_4^{\cdot-} + OH^- \rightarrow HO^{\cdot} + SO_4^{2-} \quad \text{Eq. 2}$$

Because of the sulphate radical's ($SO_4^{\bullet-}$) high redox potential, the solid-state that allows for safer handling, and its longer lifespan (40 μs) compared to the hydroxyl radical (•OH), which is less than 1 μs, PDS has been receiving significant attention in recent years in the AOP sector for treating wastewater. Activating persulfate is critical, offering diverse methodologies suited to specific applications. These methods fall into three categories: physical, chemical, and hybrid approaches (Wang and Wang, 2022). Physically, persulfate can be activated through heat (Bing and Wei, 2019; Shuchi et al., 2021; Milh et al., 2020), which induces decomposition, and ultraviolet (UV) light, which utilises photolysis to break persulfate bonds (Liu et al., 2020; Gao et al., 2021; Yan et al., 2021). Both methods are valued for their efficiency and direct activation pathways. Chemically, pH adjustment is crucial for modifying persulfate reactivity, with the optimal pH varying depending on the intended application (Matzek and Carter, 2016; Wang and Wang, 2018; Devi et al., 2016). Additionally, redox reactions, notably using ferrous ions (Fe^{2+}), serve as a potent method for chemical activation. This technique is versatile and widely used in environmental remediation (Karim et al., 2021; Liu et al., 2012; Gao et al., 2018; Rastogi et al., 2009). The hybrid method combines physical and chemical aspects, offering precise control over the activation process (Yang et al., 2021; Fang et al., 2019; Zhang et al., 2017). Among these methods, thermal activation is a straightforward yet efficient technique for activating PDS to produce reactive species. The O–O bond in PS, having a bond energy ranging between 140 and 213.3 kJ/mol, can be effectively broken at temperatures exceeding 30 °C. This process leads to the formation of $SO_4^{\bullet-}$ (as seen in Eq. (1)), which can form, indirectly, $^{\bullet}OH$ (Eq. (2)) (Wang and Wang, 2018; Sonawane et al., 2022; Yabalak et al., 2021). Recently, in the literature, the possibility of performing a dual oxidant system persulfate/peroxide ($H_2O_2/S_2O_8^{2-}$) to enhance oxidative performance has emerged as a valuable option. Dual oxidant systems in the oxidation of different pollutants from soil and groundwater, such as the combination of PDS and CaO_2, have been studied and shown to be effective (Amina et al., 2022; Qian et al., 2015; TSITONAKI et al., 2010; Masud et al., 2023; Masud et al., 2022). However, compared to the PS/CaO_2 system, the dual system involving persulfate and H_2O_2 has received less attention in the research community. While the effectiveness of the PS/CaO_2 system in removing various organic pollutants is well-documented, there is a gap in the literature regarding the detailed study of the PS/H_2O_2 system, especially its efficiency and the dynamics of its reactive species in contaminant degradation. Research towards binary PDS/H_2O_2 systems has grown in recent years, with outstanding results regarding environmental sustainability and increased oxidative activity (Qiu et al., 2022; Hilles et al., 2016; Rafiei et al., 2023). Qiu et al. (2022), for example, proposed a new activation method for PDS by combining it with H_2O_2 in a thermally activated (T-PDS). They found that this approach enhanced the remediation of refractory organic pollutants (pyrene). In their study, the introduction of H_2O_2 into the T-PDS oxidation system significantly enhanced its reactivity, leading to a 97.2% degradation of pyrene at 70 °C, and the optimal conditions were found with equal initial concentrations of PDS and H_2O_2 at 20 μM under neutral pH. Chen et al. (2020) studied the application of the binary PDS/H_2O_2 system activated by microwave in removing dinitrodiazophenol in industrial wastewater, finding a superior efficiency of this binary system compared to the single ones. This MW-PS-H_2O_2 process efficiently removed chemical oxygen demand (COD) and colour from dinitrodiazophenol industrial wastewater, achieving 73.5% COD and 98.1% colour number (CN) removal under optimized conditions of a total oxidant dose of 7.4 mM and equal PS-H_2O_2 ratios, making it a promising treatment method for this wastewater. Despite these promising results, there is a clear gap in understanding the H_2O_2/T-PDS system, particularly in optimizing its operational conditions and underlying mechanisms. This dual oxidant approach could offer a more sustainable and effective solution for wastewater treatment by reducing sludge formation—a common byproduct of traditional methods—while enhancing the removal of organic pollutants like phenols. This study hypothesized that the dual oxidant system involving H_2O_2 and T-PDS could significantly enhance the degradation efficiency of phenolic compounds, particularly phenolic compounds (PhOH) (Dargahi et al., 2023; Bazrafshan et al., 2023b; Dolatabadi et al., 2023) (Dokhani et al., 2024). the combination of RSM with chemometric tools, such as principal component analysis (PCA), enhances its predictive capabilities and facilitates a deeper understanding of AOPs. In this study, these tools proved essential for optimizing the H_2O_2/T-PDS system and advancing its application in phenolic compound degradation. By exploring the kinetics and mechanism of the H_2O_2/T-PDS system, the study sought to develop a comprehensive kinetic model that accurately described the degradation reactions.

2. Materials and methods

2.1. Chemicals

H_2O_2, potassium persulfate ($K_2S_2O_8$, ≥99.0%), titanium(IV) oxysulfate – sulfuric acid solution ($TiOSO_4$, 27–31%), potassium iodide (KI, ≥99.0%), catalase from bovine liver (CAT, 2000–5000 units/mg protein), sodium carbonate (Na_2CO_3, ≥99.5%), sodium bicarbonate ($NaHCO_3$, ≥95%), phenol (PhOH, ≥99%), sulfuric acid (H_2SO_4, 96%), sodium hydroxide (NaOH, ≥97.0%, pellets), hydrogen peroxide (H_2O_2) 30% wt, sodium carbonate (Na_2CO_3) and Folin-Ciocalteu reagent were purchased from Merck KGaA (Darmstadt, Germany) and used without further purification.

2.2. Experimental procedures

The experimental set-up consisted of a flask in which the PhOH solution (10 mg L-1) operated in batch mode. To warm the flask uniformly, it was put in a thermostatic bath. The temperature was maintained at the desired level (from 25 to 80 °C) through an electrical thermometer (VWR VWR International Srl, Milan, Italy) (figure SM1 of supporting material file (SM)). After the bath reached the temperature, the desired amount of oxidant was added. The solution was mixed through a magnetic stirrer bar, and after adding the two oxidants, the process time (set at 120 min) started. The reaction duration was fixed at 120 min. It was specifically chosen for optimization trials using RSM. During the kinetic study, samples were collected at predefined intervals (0, 15, 30, 45, 60, 75, 90, and 120 min) under optimized conditions of temperature, pH, and oxidant concentrations. Immediately after sampling, residual oxidant (H_2O_2 and $S_2O_8^{2-}$) and PhOH concentrations were analyzed to monitor the progress of the reaction and validate the kinetic model. The

study focused on optimizing four critical factors influencing the degradation efficiency of PhOH in the H_2O_2/T-PDS system: temperature, pH, H_2O_2 concentration, and $S_2O_8^{2-}$ concentration. These factors were carefully selected based on their significant role in controlling the generation of reactive oxidant species ($SO_4^{\bullet-}$ and $^{\bullet}OH$) and their impact on the degradation kinetics.

1. **Temperature (X_1)**: Temperature plays a crucial role in activating $S_2O_8^{2-}$ to produce $SO_4^{\bullet-}$ radicals. A range of 40–70 °C was investigated, as higher temperatures promote the cleavage of the peroxydisulfate bond while also enhancing the reactivity of H_2O_2. However, excessively high temperatures may lead to the rapid depletion of oxidants or energy inefficiency, making it essential to find an optimal balance.
2. **pH (X_2)**: The pH of the solution significantly affects the stability and reactivity of the oxidants. A range of 5–9 was chosen to explore both slightly acidic and neutral to alkaline conditions. Acidic pH conditions favour the formation of $SO_4^{\bullet-}$ radicals, while neutral pH conditions are more environmentally friendly and practical for real-world applications. The study aimed to identify the pH that maximizes degradation efficiency while minimizing the formation of undesirable by-products.
3. **H_2O_2 concentration (X_3)**: H_2O_2 serves as both a reactant and a source of $^{\bullet}OH$ radicals in the system. The selected range of 50–85 mg L^{-1} was based on preliminary experiments to ensure sufficient oxidant availability without introducing excessive amounts that could lead to radical scavenging or increased operational costs.
4. **$S_2O_8^{2-}$ concentration (X_4)**: $S_2O_8^{2-}$ is the primary source of $SO_4^{\bullet-}$ radicals, and its concentration directly affects the production of reactive species. A range of 50–85 mg L^{-1} was tested to determine the optimal amount needed to sustain the reaction over 120 min. Ensuring an appropriate balance between H_2O_2 and $S_2O_8^{2-}$ was critical to achieving maximum degradation efficiency without excess residual oxidants.

These four factors were systematically optimized using RSM to evaluate their individual and combined effects on PhOH removal. The quadratic model derived from the RSM analysis provided a comprehensive understanding of the interactions between these variables, enabling the identification of conditions that maximize efficiency while minimizing residual oxidants. The ranges and levels for each factor, in coded and actual values, are summarized in Table 1. The design matrix, including all experimental combinations, is detailed in Table SM1 in the supporting material (SM).

The two responses were estimated through a quadratic model according to Eq. (3):

$$Y = b_0 + \sum_{i=1}^{n} b_i X_i + \sum_{i=1}^{n} b_{ii} X_i^2 + \sum_{i=1}^{n} b_{ij} X_i X_j + \varepsilon \quad \text{Eq. 3}$$

Y is the response of PhOH removal, b0 is a constant, bi corresponds to the linear coefficient of Xi, bii is the second-order effect on regression coefficients, bij is the interaction coefficient, and ε is the statistical error. After calculating the optimal process in terms of temperature, oxidant concentration and pH, three replicates of this process were made, and the kinetics of PhOH removal were calculated and modelled. In the present study, PCA was used as a dimensionality reduction technique. PCA simplifies complex datasets by converting the original variables into a new set of orthogonal variables known as principal components. These components are distinct, uncorrelated linear combinations of the initial variables. A key characteristic of PCA is its ability to retain the intrinsic relationships among features while representing the original data's structure in a more condensed form. The principal components are prioritised according to their ability to explain the data's variance: the first principal component accounts for the largest variance, followed by the second, and so on. In this study, PCA was performed using the open-source software environment RStudio. The analysis was carried out using the '*factoextra*' package. A classical PCA was executed using the '*prcomp*' function from the same package, where data scaling was applied. Key outcomes of this analysis were derived from this procedure. For an enhanced graphical representation of the principal components (PC), the '*fviz_pca_ind*' function was used to plot the scores.

Table 1
Ranges and levels for each factor.

Variables	Code	Range and levels		
		−1	0	+1
Temperature (°C)	X_1	40	55	70
pH	X_2	5	7	9
[H_2O_2] (mg L^{-1})	X_3	50	67.5	85
[$S_2O_8^{2-}$] (mg L^{-1})	X_4	50	67.5	85

2.3. Analytical determinations

2.3.1. Residual oxidants

To measure residual $S_2O_8^{2-}$, a modified spectrophotometric method, adapted from an existing iodometric titration technique, was implemented (Liang et al., 2008). This approach involved analysing the absorbance at 352 nm of a yellow solution formed by the reaction of persulfate and iodide in a sodium bicarbonate environment, demonstrating minimal reagent matrix interference. The method's calibration curve was linear between 0 and 1 g L^{-1}. Additionally, the determination of residual H_2O_2 levels was conducted through a spectrophotometric method using titanium(IV) oxysulfate. This reagent forms a stable yellow complex with H_2O_2, detectable at 410 nm, exhibiting a linear calibration range from 0.1 to 100 mg L^{-1} (Faggiano et al., 2023c), (Fiorentino et al., 2015).

2.3.2. Phenol determination

The quantification of phenol in filtered samples was carried out employing the Folin-Ciocalteu spectrophotometric method, as described in the literature (Box, 1983). In this method, 0.25 mL of Folin-Ciocalteu's reagent was mixed with 0.75 mL of a high-concentration sodium carbonate solution (220 g L^{-1}, 2.08 M) and 5 mL of the wastewater sample. The mixture was then incubated for 60 min in a dark environment at 20 °C. Post-incubation, the resultant, blue-coloured solution's absorbance was measured using a UV–Vis spectrophotometer at 750 nm (Varian Cary® 50 UV–Vis spectrophotometer). A calibration curve was prepared using the same procedure and showed linearity in the range of 1–2 mg L^{-1}.

2.4. Kinetic model

At optimized conditions, the kinetics of H_2O_2, $S_2O_8^{2-}$ and PhOH were mathematically described. The reaction scheme outlined in Table 2 was taken into consideration for oxidation. The effect of the temperature was studied and modelled through the linearised Arrhenius equation (Eq. (3)).

$$\ln k = -\frac{E_a}{RT} + \ln A \quad \text{Eq. 3}$$

Where:
k: rate constant.
A: Arrhenius' constant.
E_a: activation energy (J mol^{-1})
R: gas constant (8.31 J K^{-1} mol^{-1})
T: temperature (K)

The Arrhenius constant was experimentally calculated. Experiments at 298, 313, 328 and 343 K were performed in the same conditions as explained in section 2.2. The reduction in $S_2O_8^{2-}$ concentration was

Table 2
Reaction schemes considered for kinetic study.

r	Reaction	k	
r_1	$S_2O_8^{2-} \xrightarrow{heat} 2SO_4^{\cdot-}$	k_1	this work
r_2	$SO_4^{\cdot-} + SO_4^{\cdot-} \rightarrow S_2O_8^{2-}$	k_2[a]	8.1x10^8 L mol^{-1} s^{-1}
r_3	$SO_4^{\cdot-} + S_2O_8^{2-} \rightarrow SO_4^{2-} + S_2O_8^{\cdot-}$	k_3[a]	1.2x10^6 L mol^{-1} s^{-1}
r_4	$SO_4^{\cdot-} + H_2O \rightarrow HSO_4^- + HO^{\cdot}$	k_4[a]	460 s^{-1}
r_5	$SO_4^{\cdot-} + HO^{\cdot} \rightarrow HSO_4^- + 0.5O_2$	k_5[a]	1x10^{10} L mol^{-1} s^{-1}
r_6	$S_2O_8^{2-} + HO^{\cdot} \rightarrow HSO_4^- + SO_4^{\cdot-} + 0.5O_2$	k_6[a]	1.2x10^7 L mol^{-1} s^{-1}
r_7	$S_2O_8^{2-} + HO^{\cdot} \rightarrow S_2O_8^{\cdot-} + HO^-$	k_7[b]	1.4x10^7 L mol^{-1} s^{-1}
r_8	$H_2O_2 + HO^{\cdot} \rightarrow H_2O + HOO^{\cdot}$	k_8[b]	3x10^7 L mol^{-1} s^{-1}
r_9	$H_2O_2 + HOO^{\cdot}/O_2^{\cdot-} \rightarrow HO^{\cdot} + H_2O/\ HO^- + O_2$	k_9[b]	3.6 L mol^{-1} s^{-1}
r_{10}	$HO^{\cdot} + HOO^{\cdot}/O_2^{\cdot-} \rightarrow H_2O/HO^- + O_2$	k_{10}[b]	1x10^{10} L mol^{-1} s^{-1}
r_{11}	$HOO^{\cdot} + HOO^{\cdot}/O_2^{\cdot-} \rightarrow H_2O_2/HOO^- + O_2$	k_{11}[b]	1x10^6 L mol^{-1} s^{-1}
r_{12}	$PhOH + SO_4^{\cdot-} \rightarrow PhOH_i$	k_{12}	this work
r_{13}	$PhOH + HO^{\cdot} \rightarrow PhOH_i$	k_{13}	this work

[a] (Ramos et al., 2023).
[b] (Li et al., 2007).

monitored for 2 h. The oxidation reactions for the model were chosen based on scavenging tests and different hypotheses from the literature (Conte et al., 2012; Giménez et al., 2023; Pignatello et al., 2006; Simunovic et al., 2011). The scheme relies on the following assumptions.

i) The oxidising species considered were $^{\bullet}$OH, SO4$^{\bullet-}$, $^{\bullet}$OOH for the H_2O_2/T-PDS process.
ii) The oxygen concentration is always in excess.

The reaction rate for each reaction was calculated as follows (Eq. (4)):

$$r_i = k_i[A][B] \quad \text{Eq. 4}$$

Where:
i: 0-13.
A, B: reagents.

The differential equations (Table 3) system was solved utilising the MATLAB 2023b function "ode15s". The model parameters were determined through the built-in optimization routine "fmincon" (Gualda-Alonso et al., 2022; Pontes et al., 2010). The results of the fitting were evaluated in terms of correlation coefficient (R^2) and root mean square error (RMSE, Eq. (5)). Kinetic experiments were conducted in triplicate, and the standard deviation of the three measurements was used to calculate the error bars displayed in the results.

$$RMSE = \sqrt{\sum_{i=1}^{n} \frac{(\hat{y}_i - y)^2}{n}} \quad \text{Eq. 5}$$

Where:
$\hat{y}_i$ = predicted values
y = measured values
n = number of observations.

Table 3
Reaction rates for the studied species.

Reaction rate expressions
$\frac{d[S_2O_8^{2-}]}{dt} = -r_1 + r_2 - r_6 - r_7$
$\frac{d[SO_4^{\cdot-}]}{dt} = r_0 - r_2 - r_3 - r_4 - r_5 + r_6$
$\frac{d[H_2O_2]}{dt} = -r_8 - r_9 + r_{11}$
$\frac{d[HO^{\cdot}]}{dt} = r_4 - r_5 - r_6 - r_7 - r_8 + r_9 - r_{10} - r_{13}$
$\frac{d[HOO^{\cdot}]}{dt} = r_8 - r_9 - r_{10} - r_{11}$
$\frac{d[PhOH]}{dt} = -r_{11} - r_{12}$

2.5. Cost analysis

Reagent and energy costs were considered to estimate the total cost per gram of PhOH removed using the H_2O_2/T-PDS system. The cost analysis was performed under the optimal experimental conditions, including the operational temperature of 70 °C, pH 5, and a reaction time of 120 min. The total reagent cost ($C_{reagents}$) was determined by calculating the mass of each oxidant consumed, specifically H_2O_2 and $K_2S_2O_8$, multiplied by their respective market prices. The molar concentrations of the oxidants were converted into mass units (m_{HP} and m_{PS}) using the known molar masses, and the total reagent cost was calculated as follows (Eq. (6)):

$$C_{reagents} = m_{HP} \cdot p_{HP} + m_{PS} \cdot p_{PS} \quad \text{Eq. 6}$$

Where p_{HP} and p_{PS} are the prices of H_2O_2 and $S_2O_8^{2-}$ per gram, respectively. The cost of H_2O_2 was estimated to be 0.003 €/g, while the cost of potassium persulfate $K_2S_2O_8$ was considered 0.005 €/g, based on current industrial-scale market prices. The total energy cost (C_{energy}) was calculated by considering the energy required to heat the solution to the operational temperature of 70 °C and maintain this temperature throughout the process duration of 120 min. The total energy consumption (E_{total}) was estimated using the following equation for heating (Eq. (7)):

$$E_{heat} = m_{solution} \cdot c_p \cdot \Delta T \quad \text{Eq. 7}$$

Where $m_{solution}$ is the mass of the solution (in kg, assuming 1 kg per liter of water), c_p is the specific heat capacity of water (4.18 J/g°C), ΔT is the temperature difference, calculated as T_{final}-$T_{initial}$ (in °C). The energy required for maintaining the temperature was estimated as an additional fraction of the heating energy to account for thermal losses. Therefore, the total energy consumed during the process was given by (Eq. (8)):

$$E_{total} = E_{heat} \cdot (1 + \alpha) \quad \text{Eq. 8}$$

where α is the estimated fraction of additional energy required to maintain the temperature, assumed to be 0.2 (or 20%). The energy cost was then calculated by converting the total energy consumption from joules to kilowatt-hours (kWh) and multiplying it by the local electricity cost per kWh ($p_{electricity}$) (Eq. (9)):

$$C_{energy} = \frac{E_{total}}{3.6 \times 10^6} \cdot p_{electricity} \quad \text{Eq. 9}$$

where 1 kWh = 3.6 × 10^6 J. The local electricity cost ($p_{electricity}$) used in the analysis was 0.103 €/kWh. The total cost per gram of PhOH removed was calculated by summing the reagent and energy costs, and dividing by the total mass of PhOH removed ($m_{PhOH\ removed}$) during the experiment (Eq. (10)):

$$C_{total} = \frac{C_{reagents} + C_{energy}}{m_{PhOH\ removed}} \quad \text{Eq. 10}$$

3. Results and discussion

3.1. RSM and PCA

This study explored the dual system of H_2O_2 and T-PDS to remove PhOH, a commonly encountered contaminant. Two statistical tools were employed to understand the process better and optimise it: PCA and RSM. PCA was utilised to simplify the dataset's complexity and visually present relationships between different variables, such as temperature, pH, and the concentrations of the oxidants (H_2O_2 and T-PDS), specifically focusing on their influence on PhOH removal efficiency. This approach helps to identify patterns and correlations between these parameters and their direct impact on PhOH degradation. Meanwhile, RSM was applied to model the process and determine optimal operating conditions by analysing how these variables affect PhOH removal

efficiency. This study aims to find the most favourable conditions for maximising PhOH removal while providing insights into the mechanisms involved. PCA was effectively utilised to explore relationships among diverse variables, including pH, oxidant dose, temperature and the percentage removal of PhOH. Two biplots were studied to explain the variance in PhOH removal better. The first (Fig. 1a) shows the comparison between Principal Components 1 and 2 (PC1 and PC2), which explains about 50% of the variance in the data. The second (Fig. 1b) compares PC1 and PC3 (again explaining about 50% of the variance). In these biplots, "L, M, H" represent the low (40 °C), medium (55 °C), and high (70 °C) temperatures, respectively.

From the comparison of PC1 and PC2, a strong positive correlation is observed between the concentrations of the two oxidants, as indicated by the slight angle between their vectors. Notably, 'pH' also shows a strong positive correlation with PC1, suggesting that variations in pH significantly influence the variance along this principal component. The dispersion of points across the biplot allows for the inference of potential relationships and groupings. The samples labelled "H" are predominantly located on the positive side of Dim2, while the "L" and "M" samples are primarily distributed along the opposing side. This pattern suggests that higher temperatures tend to improve PhOH removal, likely due to more efficient activation of the oxidants at elevated temperatures.

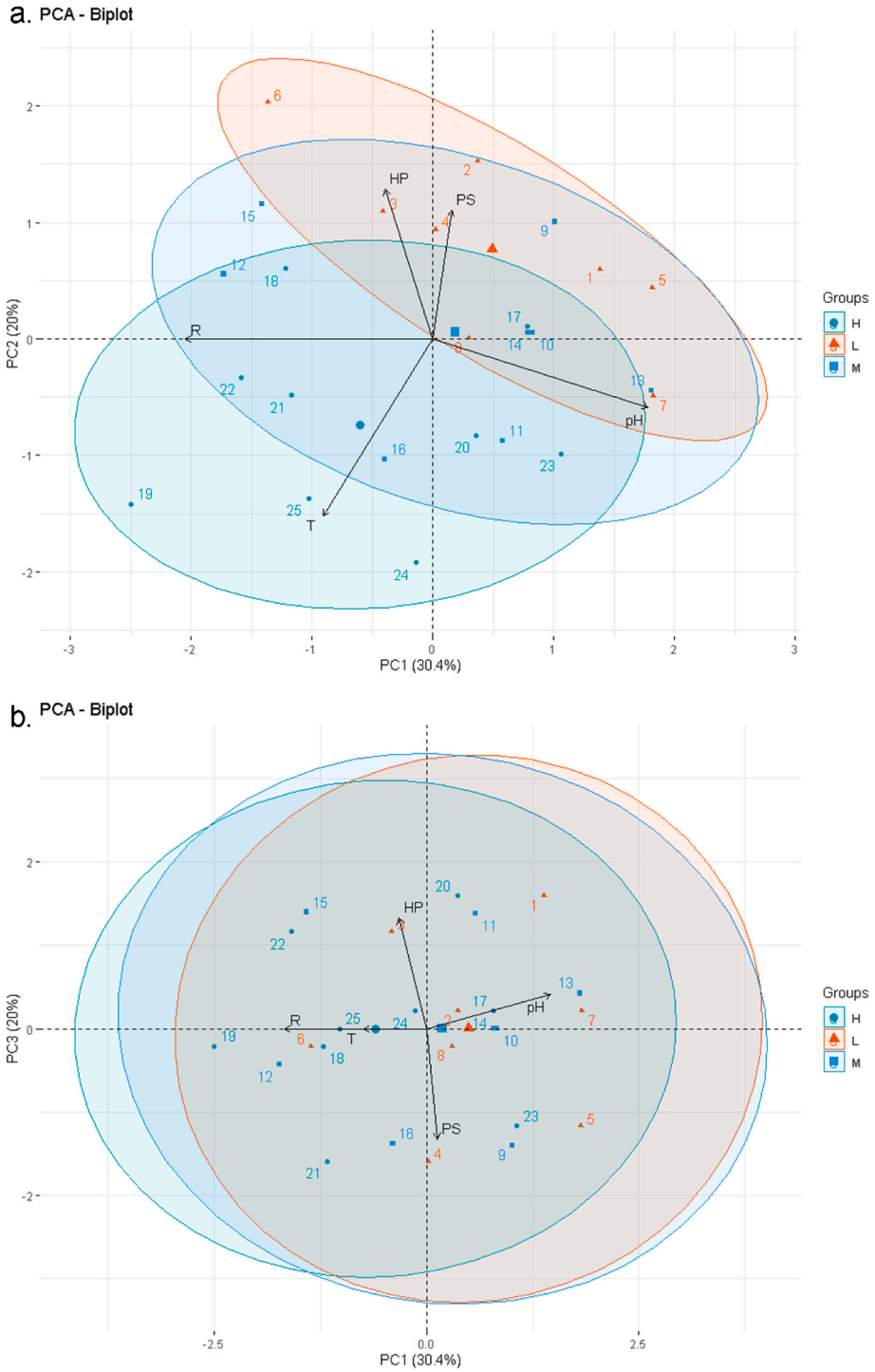

Fig. 1. PCA showing a. PC1 vs PC2 and b. PC1 vs PC3.

However, optimizing the temperature to avoid excessive consumption or degradation of the oxidants is crucial. The ellipses surrounding each group represent the variability of the data for each temperature category, with the "M" group showing the widest spread, indicating that these samples exhibit more significant variability compared to the "L" and "H" groups. This more significant variability at medium temperatures could be attributed to more complex interactions between pH, oxidant concentrations, and temperature, which affect PhOH removal differently at intermediate conditions. Since PC2 plays a crucial role in differentiating sample groups, the biplot comparing PC1 and PC3 was also examined to gain further insights that may not be visible in the PC1 vs. PC2 comparison. While PC1 provides an overview of variance, especially pH, the PC1 vs PC3 biplot reveals more detailed inter-variable relationships and sample groupings. In this comparison, PhOH removal and T temperature are positioned on the negative side of PC1, indicating an inverse relationship with the variables located on the positive side of PC1, such as pH and PS. This suggests that higher pH values and PS concentrations have a negative impact on PhOH removal efficiency, as higher levels of these variables correspond to lower PhOH removal percentages. HP forms a slight negative angle with the PC3 axis, suggesting that its contribution to the variance explained by PC3 is less pronounced than PC1. However, its role in the overall process of PhOH removal remains significant, particularly in combination with other factors such as pH and PS concentrations. On the other hand, pH forms a slight positive angle with PC1, suggesting a positive correlation with this principal component. This means that changes in pH have a more direct relationship with PC1. Still, given the inverse correlation of PhOH removal with PC1, it implies that higher pH values may not favour PhOH removal. Instead, the best PhOH removal efficiency might occur at lower pH values, as indicated by the negative positioning of PhOH removal along PC1. By comparing the PC1 and PC3 components, it is possible to observe the complex interplay between these variables. The angles and positioning of HP, PS, pH, and PhOH removal suggest that while the oxidant concentrations (HP and PS) and pH influence the process, their combined effect on PhOH removal is multifaceted and likely moderated by other conditions, such as T, which also plays a significant role. While PCA was useful for identifying linear relationships between variables such as temperature, pH, and oxidant concentrations, it does not capture non-linear interactions. Since more complex interactions influence PhOH removal, RSM was necessary to model these non-linear effects and optimise the process. RSM allowed a deeper understanding of how variables like oxidant concentrations and pH interact non-linearly to affect PhOH removal, providing the optimal conditions that PCA alone could not reveal. Fig. 2 presents the results obtained through RSM. The removal efficiency of PhOH is highest at lower pH levels and increases with higher temperatures (Fig. 2a). The red areas highlight that acidic conditions combined with elevated temperatures greatly enhance the performance of the $H_2O_2/S_2O_8^{2-}$ system. The efficiency also improves with higher concentrations of $S_2O_8^{2-}$, as indicated by the significant interaction between temperature and $S_2O_8^{2-}$ concentration (Fig. 2b). This combination creates optimal conditions for PhOH removal, likely due to more efficient radical formation. In Fig. 2c, increased H_2O_2 concentration, especially at higher temperatures, leads to greater PhOH removal, suggesting that higher temperatures boost the reactivity of H_2O_2, thus improving degradation efficiency. Fig. 2d and e depict the interaction between pH and the concentrations of oxidants. Maximum removal efficiency occurs in acidic conditions with increasing H_2O_2 concentrations (Fig. 2d), indicating that acidic environments favour the formation of highly reactive species from H_2O_2, which degrade PhOH more effectively. Fig. 2e shows that higher PhOH removal efficiency is consistently associated with lower pH, irrespective of $S_2O_8^{2-}$ concentration. This suggests that the system's sensitivity to $S_2O_8^{2-}$ concentration diminishes in acidic conditions, likely due to the potent oxidising capacity of persulfate ions in these environments. Fig. 2f illustrates the interaction between H_2O_2 and $S_2O_82^-$ concentrations. The plot shows that PhOH removal efficiency depends on the combined concentration of both oxidants, with two distinct regions of high removal efficiency—one at lower concentrations of both H_2O_2 and $S_2O_82^-$and another at higher concentrations of both chemicals. This dual peak suggests the existence of at least two distinct mechanisms or pathways that optimise PhOH removal. Radicals may form at low oxidant concentrations in optimal amounts, leading to efficient degradation without significant recombination. Although radical generation is greater at higher concentrations, recombination losses may be overcome, resulting in efficient PhOH removal despite potential side reactions. The intermediate concentration zone, where removal efficiency dips, may result from an imbalance between radical generation and recombination or scavenging processes. This indicates that while the system is robust over a range of reagent concentrations, precise control of the H_2O_2 to $S_2O_8^{2-}$ ratio is crucial for optimal performance. This flexibility in the system, coupled with its sensitivity to reagent dosages, is an essential consideration for practical applications. ANOVA results for the quadratic model and fit statistics are provided in Table SM2 and Table SM3, respectively. These findings align with results reported in previous literature. For example, Qiu et al. (2022) observed better pyrene degradation at pH < 7 in the dual H_2O_2/T-PDS system. Similarly, Chen et al. (2019) demonstrated that a system combining H_2O_2 and microwave-activated $S_2O_82^-$ achieved substantially reduced dinitrodiazophenol at pH 3.

Qiu et al., 2022 found that pyrene was better degraded at pH < 7 in the dual system HP/T-PDS (Qiu et al., 2022). Also, in the work of Chen et al., (2019) (TSITONAKI et al., 2010), the dual system formed by H_2O_2 and microwave-activated $S_2O_8^{2-}$ led to a very high reduction of dinitrodiazophenol at pH = 3.

Based on the results obtained from the quadratic model, the empirical relationships between the response and the independent variables can be described by the following equations (Eq. (11)):

$$Y_{PhOH} = 3.46 + 6.54X_1 - 12.00X_2 + 2.61X_3 - 1.00X_4 - 3.96X_1X_2 - 11.86X_1X_3 + \\ -13.04X_1X_4 + 0.99X_2X_3 - 0.32X_2X_4 + 8.02X_3X_4 + 7.62{X_1}^2 + 7.28{X_2}^2 + 16.11{X_3}^2 + 0.21{X_4}^2 \quad \text{Eq. 11}$$

The determination coefficient for PhOH removal was $R^2 = 0.9886$. The predicted and adjusted R2 differences were less than 0.2 in both cases. Notably, the Lack of Fit tests for PhOH removal (p-value: 0.1516) was insignificant compared to pure error. The Lack of Fit test assesses whether the model fits the data well. A non-significant p-value indicates that the model does not significantly deviate from the actual relationship. Concerning validating the model assumptions, the residuals plot demonstrates a slight deviation from the straight line. This indicates that the studentised residuals can be considered to follow a normal distribution. The residual plot displays a random scatter approximately centred on zero across the entire range of predicted values, indicating that the residuals are random and the variance of the observations is constant for all response values (Ribeiro et al., 2020). Moreover, no outliers were identified in either case.

3.2. Effect of temperature on $S_2O_8^{2-}$ activation

To determine the K_1 to be included in the model for Eq. (1), the effect

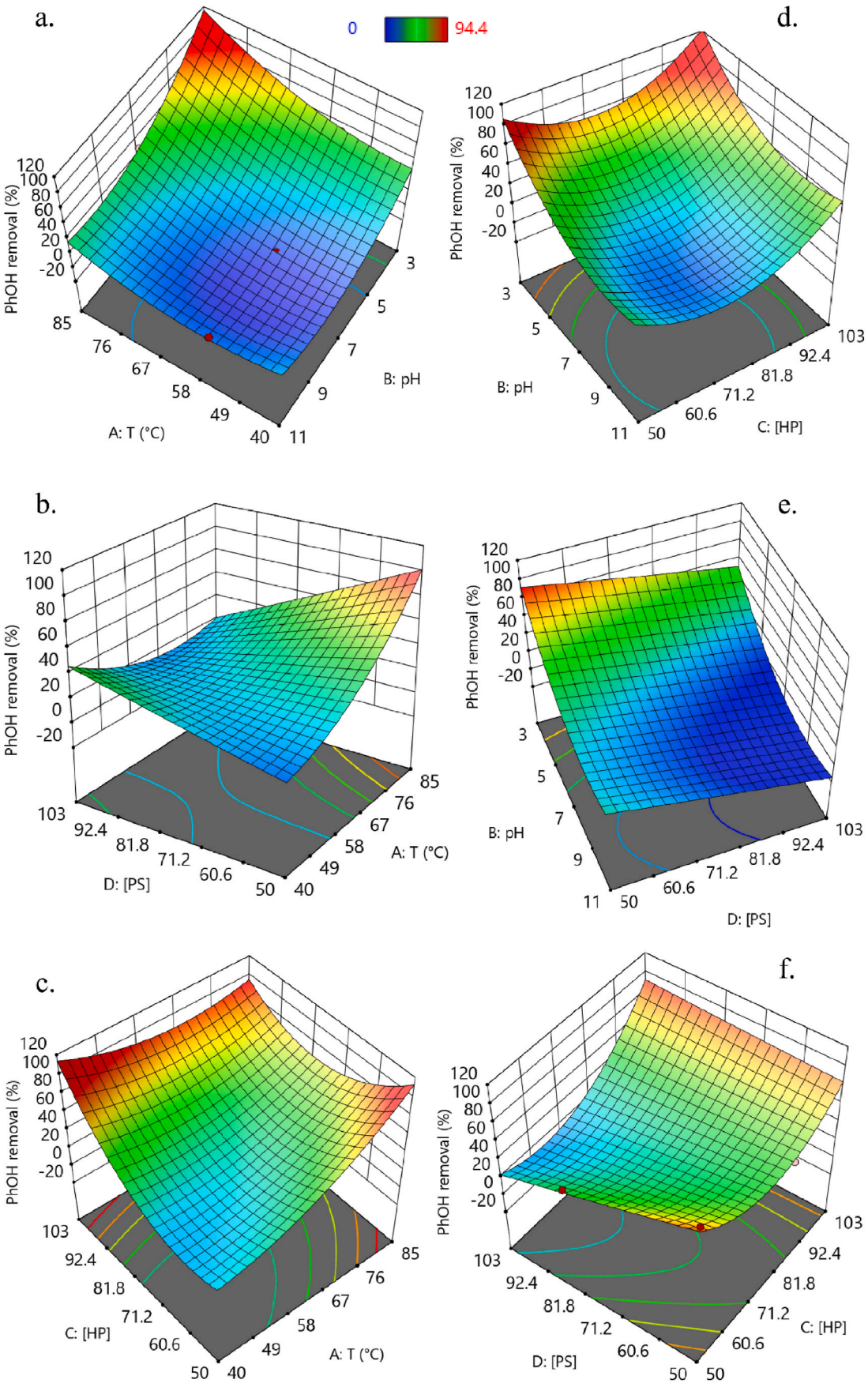

Fig. 2. 3D-surface for each factor.

of temperature on the activation of $S_2O_8^{2-}$ over varying treatment times was investigated, as shown in Fig. 3a.

The degradation kinetics of $S_2O_8^{2-}$ were studied at four distinct temperatures (Fig. 3): 30 °C (green), 40 °C (blue), 55 °C (red), and 70 °C (black). The $S_2O_8^{2-}$ concentrations are plotted over time, demonstrating an apparent acceleration in the degradation rate as the temperature increases. The data for each temperature condition were fitted with a linear regression to approximate a first-order kinetic degradation model, depicted by the dashed lines for each temperature set. The degradation is slowest at 30 °C, with $S_2O_8^{2-}$ concentration gradually decreasing over 90 min. At 70 °C, the degradation process is markedly faster, with the concentration of $S_2O_8^{2-}$ dropping steeply and going well below the concentrations observed at lower temperatures within the same time-frame. This indicates the expected increase in reaction rate with temperature, per the Arrhenius equation. The linear regressions provide the slopes that can be used to determine the Arrhenius activation energy for the degradation at each temperature, which is crucial for understanding the temperature dependence of the persulfate degradation kinetics (Fig. 3b). The E_a was equal to 168 kJ/mol. Data for temperature dependence of the rate constant are shown in Table SM4. The results agree well with previously reported values over a range of conditions (Karim et al., 2021; Macías-Vargas et al., 2021; Wang and Wang, 2018; House, 1962; Johnson et al., 2008). In this study, it's evident that the reaction rate accelerates with an increase in temperature. This is evident from the steeper decline in $S_2O_8^{2-}$ concentration at higher temperatures, aligning well with the Arrhenius equation, which relates the rate constant of a reaction to temperature. This study applies linear regression to the data at each temperature, enabling a quantitative reaction rate analysis. The study systematically compares the degradation rates across different temperatures by fitting the data to a first-order kinetic model. The slopes derived from these regressions are crucial for calculating the Arrhenius activation energy (Ea) for the degradation process. The determined mean Ea value of 168 kJ/mol indicates a significant energy barrier for $S_2O_8^{2-}$ degradation, which is crucial for understanding its temperature-dependent behaviour. Moreover, the consistency of these findings with previously reported values underscores the reliability of the results and suggests the soundness of the experimental design and methodology. Understanding the degradation kinetics of $S_2O_8^{2-}$ at various temperatures is vital for practical applications, especially in environmental chemistry and industrial processes where persulfates are commonly used.

3.3. Kinetic study

This study investigated the kinetic analysis of phenol degradation under the optimized conditions as determined by the factorial design and RSM. The data showcases the degradation kinetics of phenol when treated with the H_2O_2/T-PDS system at the best molar ratio (mol H_2O_2/mol $S_2O_8^{2-}$: 1/6), activation temperature (70 °C), and pH level (5). The fitting of this experimental data to our kinetic model is also illustrated (Fig. 4), providing a quantifiable measure of the system's efficiency.

The kinetic profile of PhOH degradation is observed to follow a non-linear decay, which suggests a reaction mechanism that may involve multiple steps or a change in the rate-determining step as the reaction progresses. The experimental points for each reactant show a decreasing trend, indicating the consumption of PhOH, $S_2O_8^{2-}$, and H_2O_2 over time. The dashed lines represent the model fits, which correspond well with the experimental data, implying that the kinetic model can adequately describe the system's behaviour. Notably, the degradation kinetics of PhOH demonstrates a pronounced decay, indicative of a robust reaction rate. This decay is accentuated at initial time points, signifying a rapid consumption of PhOH that may correlate with a high initial concentration of reactive oxidant species. In fact, after the first 15 min of the reaction, PhOH concentration decreased by about 38%; after 30 min, it decreased by 15 % at 45 and 60 min. As the reaction proceeds, the rate of PhOH degradation appears to decelerate, possibly due to the depletion of oxidants or the accumulation of reaction intermediates that may act as inhibitors or alternate reactants. In fact, from 75 to 120 min. The residual PhOH concentration remained almost constant. The final PhOH

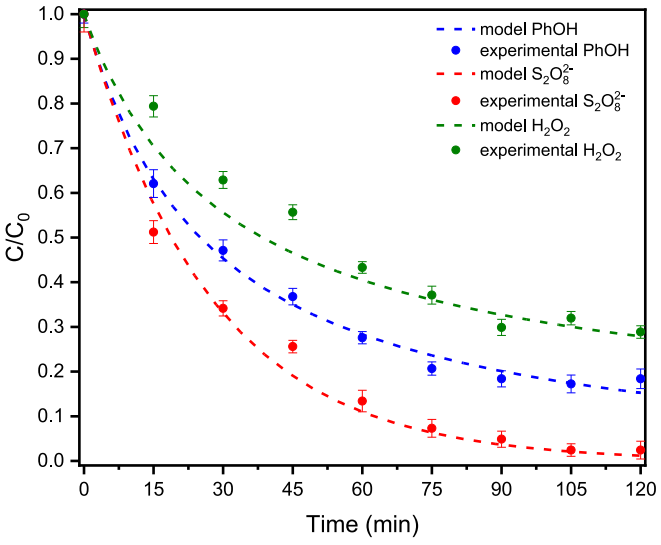

Fig. 4. Degradation kinetics at the optimized conditions and fitted kinetic model. Green data show the H_2O_2 consumption during the experiment; red data show the $S_2O_8^{2-}$ consumption, and blue data show the PhOH degradation.

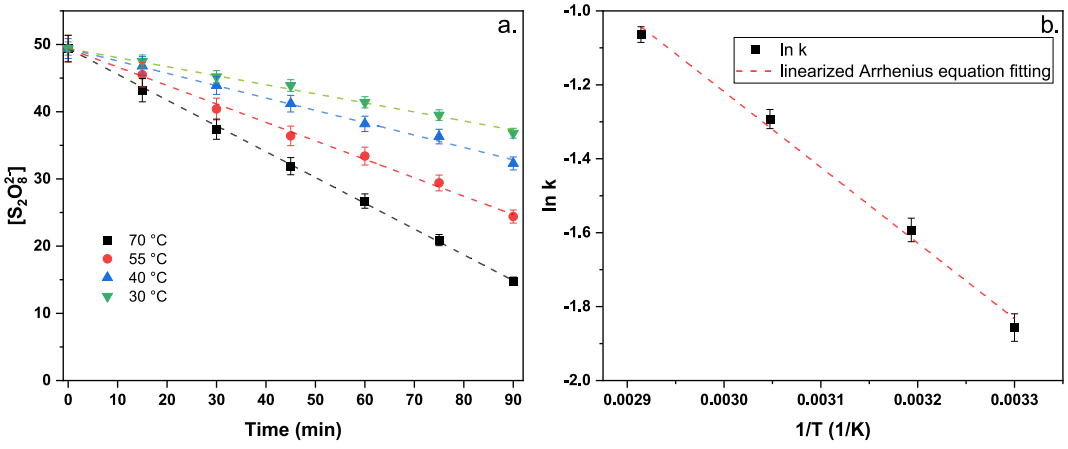

Fig. 3. – degradation kinetics of $S_2O_8^{2-}$ at different temperatures (a.) and linearised Arrhenius equation fitting (b.).

concentration was 1.2 mg L^{-1}, with a degradation of about 89%. The kinetic curves for $S_2O_8^{2-}$ and H_2O_2 display distinct slopes, reflecting their consumption rates and possible differences in reactivity towards PhOH. $S_2O_8^{2-}$, a known source of $SO_4^{\bullet-}$ radicals upon activation, shows a steady decline in concentration, hinting at its continual involvement in generating reactive species. H_2O_2, on the other hand, exhibits a slightly different kinetic profile, potentially due to its dual role as a reactant and a radical generator in the system. The coefficient of determination (R^2) and the root mean square error (RMSE) for PhOH, $S_2O_8^{2}$, and H_2O_2 indicate the model's accuracy and precision in fitting the experimental data. For PhOH and $S_2O_8^{2-}$, the R^2 values are both at 0.99, demonstrating an excellent fit where the model captures 99% of the variability in the experimental data. The RMSE values for these two are relatively low, at 0.017 and 0.033, respectively, indicating that the average deviations of the predicted concentrations from the observed values are minimal. H_2O_2 has a slightly lower R^2 of 0.98, which is still considered a very good fit, and a higher RMSE of 0.046, suggesting a bit more variability in the model's predictions for H_2O_2 concentrations compared to the other two reactants. Overall, these parameters confirm that the kinetic model is well-constructed and reliable, providing high confidence in its predictive ability for the degradation kinetics of the system under study. The application of the kinetic model in this study highlights a robust correlation between the degradation mechanism of PhOH and the consumption of reactive oxidants. The dual oxidant system's performance aligns closely with the findings of Hilles et al., who demonstrated significant improvements in the removal of COD and ammonia nitrogen (NH_3-N) using sodium persulfate and hydrogen peroxide for landfill leachate treatment. Hilles et al. attributed this enhancement to the synergistic generation of sulphate ($SO_4^{\bullet-}$) and hydroxyl ($^{\bullet}OH$) radicals, similar to the mechanism proposed in this study. While their system was optimized at an alkaline pH of 11, the focus on circumneutral pH conditions in this work provides a notable advantage in environmental compatibility, reducing the need for extensive chemical adjustments (Hilles et al., 2016). Notably, the initial rapid degradation of PhOH aligns with other findings in literature regarding AOPs, such as heterogeneous Fenton and electrochemical systems. For example, Shokoohi et al. demonstrated that a Fenton-like process using magnetic nanoparticles can achieve high efficiency in degrading Bisphenol A, emphasizing the role of optimized reaction conditions, similar to the current study's focus on pH and oxidant dosages (Shokoohi et al., 2018). Similarly, Dargahi et al. reported on the high removal efficiencies of 2, 4-Dinitrophenol using a 3D/SEC system, which also leveraged statistical optimization techniques for process refinement (Dargahi et al., 2022). In contrast to traditional electrochemical degradation methods, the dual oxidant system studied here provides a synergistic approach by integrating hydrogen peroxide and thermally activated persulfate. This approach mirrors the advancements seen in hybrid systems like those described by Samarghandi et al., where granular activated carbon significantly enhanced pollutant degradation (Samarghandi et al., 2021a). Moreover, the integration of chemometric tools such as RSM and PCA enabled the precise optimization of reaction conditions. This methodology is in alignment with the central composite design (CCD) approaches used in studies like those on the degradation of 2,4-DNT, where RSM proved instrumental in identifying the interactions and quadratic effects of independent variables (Dargahi et al., 2022). To provide a deeper understanding of the degradation mechanism of phenol in the H_2O_2/T-PDS system, the proposed pathway is depicted in Fig. 5. Upon thermal activation, $S_2O_8^{2-}$ undergoes homolytic cleavage, producing two sulphate radicals ($SO_4^{\bullet-}$) with a high redox potential (2.5–3.1 V). These radicals initiate the oxidation of phenol via direct attack on the aromatic ring, forming phenolic radicals that undergo rapid hydroxylation, leading to intermediates such as catechol, hydroquinone, and benzoquinone. The hydroxyl radicals ($^{\bullet}OH$), generated concurrently by H_2O_2 decomposition and $SO_4^{\bullet-}$ interaction with water molecules, further oxidize these intermediates. The synergistic action of $SO_4^{\bullet-}$ and $^{\bullet}OH$ promotes successive oxidation steps, including aromatic ring cleavage, forming smaller aliphatic organic acids such as formic acid and oxalic acid. These acids are subsequently oxidized through decarboxylation reactions, ultimately producing CO_2, sulphate ions (SO_4^{2-}), and water. The overall process highlights the complementary roles of $SO_4^{\bullet-}$ and $^{\bullet}OH$: $SO_4^{\bullet-}$ acts as a selective oxidant, primarily targeting aromatic structures, while $^{\bullet}OH$ contributes to non-selective oxidation of intermediate species, accelerating the overall mineralization process. This proposed mechanism aligns with the observed kinetic behaviour and is supported by existing literature, demonstrating the efficiency of the H_2O_2/T-PDS system in achieving high degradation rates with minimal by-product formation under optimized conditions.

3.4. Cost analysis

A detailed cost analysis was performed to assess the economic feasibility of the H_2O_2/T-PDS system for the removal of PhOH from wastewater. The system was evaluated under optimal conditions, including a temperature of 70 °C, a pH of 5, and a treatment duration of 120 min. These parameters were chosen based on their effectiveness in maximising phenol degradation while maintaining low reagent consumption. The analysis revealed that the total cost for treating 1 m^3 of wastewater was € 6.86/m^3. This amount includes reagent and energy costs, reflecting the system's efficiency in terms of operational expenses. Furthermore, the cost per gram of PhOH removed was calculated to be € 0.77/g, providing a direct measure of the system's economic efficiency. This cost is especially relevant for industrial applications, where

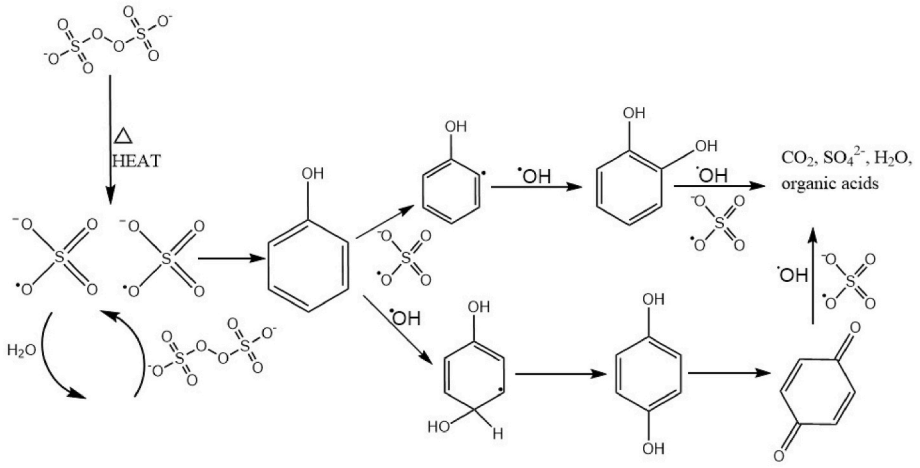

Fig. 5. – Proposed mechanism for PhOH degradation through H_2O_2/T-PDS system.

Table 4
Optimized operational conditions for the H_2O_2/T-PDS system and their corresponding cost contributions.

Parameter	Optimized condition	Unit	Cost contribution (€)
Temperature	70	°C	0.50
pH	5	–	0.30
H_2O_2 concentration	67.5	mg L^{-1}	3.00
$S_2O_8^{2-}$ concentration	67.5	mg L^{-1}	2.50
Reaction time	120	min	0.50
Mixing (stirring)	300	rpm	0.06
Total Treatment cost	–	€ m^{-3}	6.86
Cost per gram of PhOH removed	–	€ g^{-1}	0.77

minimizing the expense of removing each gram of contaminant is critical. The affordability of the reagents, coupled with a moderate energy requirement, contributes to this low cost per gram, making the system suitable for large-scale operations. In addition, it is essential to note that the relationship between phenol concentration and its COD was accounted for (with 1 g L^{-1} of phenol corresponding to a COD of 2.44 g O_2 L^{-1}). This allows for an easy estimation of the system's performance regarding organic load reduction. A key advantage of this process is that it eliminates sludge production, significantly reducing the costs typically associated with sludge management and disposal in conventional advanced wastewater treatment methods. The absence of sludge formation simplifies the overall treatment process and reduces the environmental impact, enhancing the system's appeal for industrial-scale applications. Overall, the H_2O_2/T-PDS system is a cost-effective and scalable solution for treating phenolic compounds in wastewater, offering significant savings in reagent and sludge management costs while delivering high removal efficiencies. Table 4 summarizes the optimized operational conditions for the H_2O_2/T-PDS system and their corresponding cost contributions.

4. Study limitations

The study explored the potential of the H_2O_2/T-PDS system for degrading phenolic compounds, yielding promising results. However, certain limitations should be noted. The experimental setup utilised a controlled environment with a model pollutant (PhOH), which simplifies the complexities of real wastewater containing diverse contaminants and fluctuating conditions. Additionally, while the study highlights the efficiency of the system, the scalability to industrial applications and the evaluation of operational challenges, such as energy consumption and by-product management, require further investigation. Long-term assessments of system performance, including the potential accumulation of intermediates or changes in efficiency over repeated cycles, were not conducted. Addressing these aspects in future research will strengthen the applicability and reliability of the findings.

5. Conclusions

This study highlights the significant potential of the H_2O_2/T-PDS system as an innovative approach for the degradation of phenolic compounds, specifically PhOH, in wastewater treatment. By systematically optimizing critical treatment parameters through RSM and PCA, the study identified the optimal conditions as 70 °C, pH 5, and an H_2O_2/$S_2O_8^{2-}$ molar ratio of 1:6. These conditions enabled 89% degradation of PhOH, reducing its concentration from 10 mg L^{-1}–1.2 mg L^{-1} within 120 min, demonstrating the system's remarkable efficiency. The kinetic analysis provided critical insights into the reaction mechanism, revealing a non-linear degradation profile. The rapid initial decay of PhOH concentration, attributed to the high availability of reactive oxidant species, was followed by a slower phase likely caused by oxidant depletion and the accumulation of reaction intermediates. The developed kinetic model, validated through high R^2 values (0.99 for PhOH and $S_2O_8^{2-}$, 0.98 for H_2O_2) and low RMSE values, underscores the robustness and reliability of the system. The distinct consumption profiles of $S_2O_8^{2-}$ and H_2O_2 highlight the synergistic action of $SO_4^{\bullet-}$ and $^{\bullet}OH$ radicals in driving the degradation process, emphasizing the complex interactions within the dual oxidant system. In addition to its technical performance, the economic analysis demonstrates the practicality of the H_2O_2/T-PDS system for industrial applications, with a treatment cost of €6.86 per m^3 of wastewater and €0.77 per gram of PhOH removed. The elimination of sludge formation not only reduces operational costs but also addresses a significant challenge in conventional wastewater treatment methods, enhancing the overall sustainability of the system. Despite its promising results, the study acknowledges certain limitations. Long-term operational evaluations and assessments under real-world conditions are necessary to confirm the system's scalability and reliability. Future research should also explore the system's applicability to a wider range of pollutants and investigate strategies to manage potential by-products, ensuring compliance with environmental safety standards.

CRediT authorship contribution statement

Antonio Faggiano: Writing – original draft, Methodology, Investigation, Formal analysis. **Ana B. Martínez-Piernas:** Methodology, Formal analysis. **Maria Ricciardi:** Writing – review & editing, Methodology. **Oriana Motta:** Writing – review & editing, Supervision, Conceptualization. **Antonino Fiorentino:** Writing – review & editing, Supervision, Project administration, Conceptualization. **Antonio Proto:** Supervision, Funding acquisition, Conceptualization.

Declaration of competing interest

The authors declare that they have no known competing financial interests or personal relationships that could have appeared to influence the work reported in this paper.

Acknowledgements

This work was financially supported by the research fund "FRB", University of Salerno (300389FRB22CAROT_01), Italy.

Appendix A. Supplementary data

Supplementary data to this article can be found online at https://doi.org/10.1016/j.jenvman.2024.123957.

Data availability

Data will be made available on request.

References

Akbari, M.Z., Xu, Y., Lu, Z., Peng, L., 2021. Review of antibiotics treatment by advance oxidation processes. Environmental Advances 5, 100111. https://doi.org/10.1016/j.envadv.2021.100111.

Almasi, A., Mahmoudi, M., Mohammadi, M., Dargahi, A., Biglari, H., 2021. Optimizing biological treatment of petroleum industry wastewater in a facultative stabilization pond for simultaneous removal of carbon and phenol. Toxin Rev. 40, 189–197. https://doi.org/10.1080/15569543.2019.1573433.

Amina, Abbas, Q., Shakoor, A., Naushad, M., Yousaf, B., 2022. In-situ oxidative degradation of sulfamethoxazole by calcium peroxide/persulfate dual oxidant system in water and soil. Process Saf. Environ. Protect. 164, 696–705. https://doi.org/10.1016/j.psep.2022.06.052.

Attar, S.B.-E., Soriano-Molina, P., Pichel, N., París-Reche, A., Plaza-Bolaños, P., Agüera, A., Pérez, J.A.S., 2023. Continuous flow operation of solar photo-Fenton fused with NaOCl as a novel tertiary treatment. J. Hazard Mater. 460, 132354. https://doi.org/10.1016/j.jhazmat.2023.132354.

Bazrafshan, E., Mohammadi, L., Zarei, A.A., Mosafer, J., Zafar, M.N., Dargahi, A., 2023a. Optimization of the photocatalytic degradation of phenol using superparamagnetic

iron oxide (Fe3O4) nanoparticles in aqueous solutions. RSC Adv. 13, 25408–25424. https://doi.org/10.1039/D3RA03612J.
Bazrafshan, E., dahmardeh, Z., Mohammadi, L., NadeemZafar, M., Dargahi, A., Pirdadeh, F., 2023b. Synthesis of magnesium oxide nanoparticles and its application for photocatalytic removal of furfural from aqueous media: optimization using response surface methodology. Arab. J. Chem. 16, 104998. https://doi.org/10.1016/j.arabjc.2023.104998.
Bing, W., Wei, W., 2019. Degradation phenol wastewater by heating activated persulfate. IJEMA 7, 14. https://doi.org/10.11648/j.ijema.20190701.12.
Box, J.D., 1983. Investigation of the Folin-Ciocalteau phenol reagent for the determination of polyphenolic substances in natural waters. Water Res. 17, 511–525. https://doi.org/10.1016/0043-1354(83)90111-2.
Brillas, E., Garcia-Segura, S., 2020. Benchmarking recent advances and innovative technology approaches of Fenton, photo-Fenton, electro-Fenton, and related processes: a review on the relevance of phenol as model molecule. Separation and Purification Technology 237, 116337. https://doi.org/10.1016/j.seppur.2019.116337.
Chen, W., Luo, Y., Ran, G., Li, Q., 2020. Microwave-induced persulfate-hydrogen peroxide binary oxidant process for the treatment of dinitrodiazophenol industrial wastewater. Chem. Eng. J. 382, 122803. https://doi.org/10.1016/j.cej.2019.122803.
Conte, L.O., Farias, J., Albizzati, E.D., Alfano, O.M., 2012. Photo-fenton degradation of the herbicide 2,4-dichlorophenoxyacetic acid in laboratory and solar pilot-plant reactors. Ind. Eng. Chem. Res. 51, 4181–4191. https://doi.org/10.1021/ie2023228.
Dargahi, A., Rahimzadeh Barzoki, H., Vosoughi, M., Ahmad Mokhtari, S., 2022. Enhanced electrocatalytic degradation of 2,4-Dinitrophenol (2,4-DNP) in three-dimensional sono-electrochemical (3D/SEC) process equipped with Fe/SBA-15 nanocomposite particle electrodes: degradation pathway and application for real wastewater. Arab. J. Chem. 15, 103801. https://doi.org/10.1016/j.arabjc.2022.103801.
Dargahi, A., Samarghandi, M.R., Shabanloo, A., Mahmoudi, M.M., Nasab, H.Z., 2023. Statistical modeling of phenolic compounds adsorption onto low-cost adsorbent prepared from aloe vera leaves wastes using CCD-RSM optimization: effect of parameters, isotherm, and kinetic studies. Biomass Conv. Bioref. 13, 7859–7873. https://doi.org/10.1007/s13399-021-01601-y.
Devi, P., Das, U., Dalai, A.K., 2016. In-situ chemical oxidation: principle and applications of peroxide and persulfate treatments in wastewater systems. Sci. Total Environ. 571, 643–657. https://doi.org/10.1016/j.scitotenv.2016.07.032.
Dokhani, A., kheirkhah, B., Kalantar-Neyestanaki, D., Rokhbakhsh-Zamin, F., Dolatabadi, M., Ahmadzadeh, S., 2024. Removal of Staphylococcus aureus using electro-fenton, UV/H2O2, and combination of electro-fenton and UV/H2O2 processes; optimization of operational parameters. Appl. Water Sci. 14, 100. https://doi.org/10.1007/s13201-024-02151-0.
Dolatabadi, M., Ehrampoush, M.H., Pournamdari, M., Ebrahimi, A.A., Fallahzadeh, H., Ahmadzadeh, S., 2023. Enhanced electrocatalytic elimination of fenitrothion, trifluralin, and chlorothalonil from groundwater and industrial wastewater using modified Cu-PbO2 electrode. J. Mol. Liq. 379, 121706. https://doi.org/10.1016/j.molliq.2023.121706.
Faggiano, A., Ricciardi, M., Fiorentino, A., Cucciniello, R., Motta, O., Rizzo, L., Proto, A., 2022. Combination of foam fractionation and photo-Fenton like processes for greywater treatment. Separation and Purification Technology 293, 121114. https://doi.org/10.1016/j.seppur.2022.121114.
Faggiano, A., De Carluccio, M., Fiorentino, A., Ricciardi, M., Cucciniello, R., Proto, A., Rizzo, L., 2023a. Photo-Fenton like process as polishing step of biologically co-treated olive mill wastewater for phenols removal. Separation and Purification Technology 305, 122525. https://doi.org/10.1016/j.seppur.2022.122525.
Faggiano, A., Ricciardi, M., Motta, O., Fiorentino, A., Proto, A., 2023b. Greywater treatment for reuse: effect of combined foam fractionation and persulfate-iron based fenton process in the bacterial removal and degradation of organic matter and surfactants. J. Clean. Prod., 137792
Faggiano, A., Ricciardi, M., Motta, O., Fiorentino, A., Proto, A., 2023c. Greywater treatment for reuse: effect of combined foam fractionation and persulfate-iron based fenton process in the bacterial removal and degradation of organic matter and surfactants. J. Clean. Prod. 415, 137792. https://doi.org/10.1016/j.jclepro.2023.137792.
Fang, Z., Huang, R., Chelme-Ayala, P., Shi, Q., Xu, C., Gamal El-Din, M., 2019. Comparison of UV/Persulfate and UV/H2O2 for the removal of naphthenic acids and acute toxicity towards Vibrio fischeri from petroleum production process water. Sci. Total Environ. 694, 133686. https://doi.org/10.1016/j.scitotenv.2019.133686.
Fiorentino, A., Ferro, G., Alferez, M.C., Polo-López, M.I., Fernández-Ibañez, P., Rizzo, L., 2015. Inactivation and regrowth of multidrug resistant bacteria in urban wastewater after disinfection by solar-driven and chlorination processes. J. Photochem. Photobiol. B Biol. 148, 43–50. https://doi.org/10.1016/j.jphotobiol.2015.03.029.
Fiorentino, A., Lofrano, G., Cucciniello, R., Carotenuto, M., Motta, O., Proto, A., Rizzo, L., 2021. Disinfection of roof harvested rainwater inoculated with E. coli and Enterococcus and post-treatment bacterial regrowth: conventional vs solar driven advanced oxidation processes. Sci. Total Environ. 801, 149763. https://doi.org/10.1016/j.scitotenv.2021.149763.
Fiorentino, A., Soriano-Molina, P., Abeledo-Lameiro, M.J., de la Obra, I., Proto, A., Polo-López, M.I., Pérez, J.A.S., Rizzo, L., 2022. Neutral (Fe3+-NTA) and acidic (Fe2+) pH solar photo-Fenton vs chlorination: effective urban wastewater disinfection does not mean control of antibiotic resistance. J. Environ. Chem. Eng. 10, 108777. https://doi.org/10.1016/j.jece.2022.108777.
Gao, F., Li, Y., Xiang, B., 2018. Degradation of bisphenol A through transition metals activating persulfate process. Ecotoxicol. Environ. Saf. 158, 239–247. https://doi.org/10.1016/j.ecoenv.2018.03.035.
Gao, Y., Zhou, J., Zhang, J., Li, C., Gao, N., Yin, D., 2021. Factors affecting UV/persulfate treatment of phenacetin and its disinfection byproduct formation potential. Separation and Purification Technology 256, 117819. https://doi.org/10.1016/j.seppur.2020.117819.
Giménez, B.N., Conte, L.O., Audino, F., Schenone, A.V., Graells, M., Alfano, O.M., Pérez-Moya, M., 2023. Kinetic model of photo-Fenton degradation of paracetamol in an annular reactor: main reaction intermediates and cytotoxicity studies. Catal. Today 413–415, 113958. https://doi.org/10.1016/j.cattod.2022.11.019.
Gualda-Alonso, E., Soriano-Molina, P., García Sánchez, J.L., Casas López, J.L., Sánchez Pérez, J.A., 2022. Mechanistic modeling of solar photo-Fenton with Fe3+-NTA for microcontaminant removal. Appl. Catal. B Environ. 318, 121795. https://doi.org/10.1016/j.apcatb.2022.121795.
Hilles, A.H., Abu Amr, S.S., Hussein, R.A., El-Sebaie, O.D., Arafa, A.I., 2016. Performance of combined sodium persulfate/H2O2 based advanced oxidation process in stabilized landfill leachate treatment. J. Environ. Manag. 166, 493–498. https://doi.org/10.1016/j.jenvman.2015.10.051.
House, D.A., 1962. Kinetics and mechanism of oxidations by peroxydisulfate. Chem. Rev. 62, 185–203. https://doi.org/10.1021/cr60217a001.
Iakovides, I.C., Manoli, K., Karaolia, P., Michael-Kordatou, I., Manaia, C.M., Fatta-Kassinos, D., 2021. Reduction of antibiotic resistance determinants in urban wastewater by ozone: emphasis on the impact of wastewater matrix towards the inactivation kinetics, toxicity and bacterial regrowth. J. Hazard Mater. 420, 126527. https://doi.org/10.1016/j.jhazmat.2021.126527.
Johnson, R.L., Tratnyek, P.G., Johnson, R.O., 2008. Persulfate persistence under thermal activation conditions. Environ. Sci. Technol. 42, 9350–9356. https://doi.org/10.1021/es8019462.
Karim, A.V., Jiao, Y., Zhou, M., Nidheesh, P.V., 2021. Iron-based persulfate activation process for environmental decontamination in water and soil. Chemosphere 265, 129057. https://doi.org/10.1016/j.chemosphere.2020.129057.
Li, K., Stefan, M.I., Crittenden, J.C., 2007. Trichloroethene degradation by UV/H2O2 advanced oxidation process: product study and kinetic modeling. Environ. Sci. Technol. 41, 1696–1703. https://doi.org/10.1021/es0607638.
Liang, C., Huang, C.-F., Mohanty, N., Kurakalva, R.M., 2008. A rapid spectrophotometric determination of persulfate anion in ISCO. Chemosphere 73, 1540–1543. https://doi.org/10.1016/j.chemosphere.2008.08.043.
Liu, C.S., Shih, K., Sun, C.X., Wang, F., 2012. Oxidative degradation of propachlor by ferrous and copper ion activated persulfate. Sci. Total Environ. 416, 507–512. https://doi.org/10.1016/j.scitotenv.2011.12.004.
Liu, X., Liu, Y., Lu, S., Wang, Z., Wang, Y., Zhang, G., Guo, X., Guo, W., Zhang, T., Xi, B., 2020. Degradation difference of ofloxacin and levofloxacin by UV/H2O2 and UV/PS (persulfate): efficiency, factors and mechanism. Chem. Eng. J. 385, 123987. https://doi.org/10.1016/j.cej.2019.123987.
Macías-Vargas, J.-A., Campos-Mañas, M.C., Agüera, A., Sánchez Pérez, J.A., Ramírez-Zamora, R.-M., 2021. Enhanced activated persulfate oxidation of ciprofloxacin using a low-grade titanium ore under sunlight: influence of the irradiation source on its transformation products. Environ. Sci. Pollut. Res. 28, 24008–24022. https://doi.org/10.1007/s11356-020-11564-8.
Masud, M.A.A., Kim, D.G., Shin, W.S., 2022. Highly efficient degradation of phenolic compounds by Fe(II)-activated dual oxidant (persulfate/calcium peroxide) system. Chemosphere 299, 134392. https://doi.org/10.1016/j.chemosphere.2022.134392.
Masud, M.A.A., Shin, W.S., Kim, D.G., 2023. Degradation of phenol by ball-milled activated carbon (ACBM) activated dual oxidant (persulfate/calcium peroxide) system: effect of preadsorption and sequential injection. Chemosphere 312, 137120. https://doi.org/10.1016/j.chemosphere.2022.137120.
Matzek, L.W., Carter, K.E., 2016. Activated persulfate for organic chemical degradation: a review. Chemosphere 151, 178–188. https://doi.org/10.1016/j.chemosphere.2016.02.055.
Milh, H., Schoenaers, B., Stesmans, A., Cabooter, D., Dewil, R., 2020. Degradation of sulfamethoxazole by heat-activated persulfate oxidation: elucidation of the degradation mechanism and influence of process parameters. Chem. Eng. J. 379, 122234. https://doi.org/10.1016/j.cej.2019.122234.
Nidheesh, P.V., Zhou, M., Oturan, M.A., 2018. An overview on the removal of synthetic dyes from water by electrochemical advanced oxidation processes. Chemosphere 197, 210–227. https://doi.org/10.1016/j.chemosphere.2017.12.195.
Pignatello, J.J., Oliveros, E., MacKay, A., 2006. Advanced oxidation processes for organic contaminant destruction based on the fenton reaction and related chemistry. Crit. Rev. Environ. Sci. Technol. 36, 1–84. https://doi.org/10.1080/10643380500326564.
Pontes, R.F.F., Moraes, J.E.F., Machulek, A., Pinto, J.M., 2010. A mechanistic kinetic model for phenol degradation by the Fenton process. J. Hazard Mater. 176, 402–413. https://doi.org/10.1016/j.jhazmat.2009.11.044.
Qian, Y., Zhou, X., Zhang, Y., Sun, P., Zhang, W., Chen, J., Guo, X., Zhang, X., 2015. Performance of α-methylnaphthalene degradation by dual oxidant of persulfate/calcium peroxide: implication for ISCO. Chem. Eng. J. 279, 538–546. https://doi.org/10.1016/j.cej.2015.05.053.
Qiu, R., Zhang, P., Feng, G., Ni, X., Miao, Z., Wei, L., Sun, H., 2022. Enhanced thermal activation of persulfate by coupling hydrogen peroxide for efficient degradation of pyrene. Chemosphere 303, 135057. https://doi.org/10.1016/j.chemosphere.2022.135057.
Rafiei, Z., Marioryad, H., Jamshidi, A., Hassani, G., Naghmachi, M., 2023. Investigation of hospital wastewater treatment using the UV/H2O2/S2O82- process as a combined AOP method. Int. J. Environ. Anal. Chem. 0, 1–12. https://doi.org/10.1080/03067319.2023.2198090.
Ramos, B., Ferreira, L.B., Palharim, P.H., Metolina, P., Gusmão, C. de A., Teixeira, A.C.S. C., 2023. A continuous photo-Fenton-like process using persulfate salts for the degradation of acetaminophen under solar irradiation at circumneutral pH.

Chemical Engineering Journal Advances 14, 100473. https://doi.org/10.1016/j.ceja.2023.100473.

Rastogi, A., Al-Abed, S.R., Dionysiou, D.D., 2009. Effect of inorganic, synthetic and naturally occurring chelating agents on Fe(II) mediated advanced oxidation of chlorophenols. Water Res. 43, 684–694. https://doi.org/10.1016/j.watres.2008.10.045.

Ribeiro, J.P., Marques, C.C., Portugal, I., Nunes, M.I., 2020. Fenton processes for AOX removal from a kraft pulp bleaching industrial wastewater: optimisation of operating conditions and cost assessment. J. Environ. Chem. Eng. 8, 104032. https://doi.org/10.1016/j.jece.2020.104032.

Samarghandi, M.R., Dargahi, A., Rahmani, A., Shabanloo, A., Ansari, A., Nematollahi, D., 2021a. Application of a fluidized three-dimensional electrochemical reactor with Ti/SnO2–Sb/β-PbO2 anode and granular activated carbon particles for degradation and mineralization of 2,4-dichlorophenol: process optimization and degradation pathway. Chemosphere 279, 130640. https://doi.org/10.1016/j.chemosphere.2021.130640.

Samarghandi, M.R., Ansari, A., Dargahi, A., Shabanloo, A., Nematollahi, D., Khazaei, M., Nasab, H.Z., Vaziri, Y., 2021b. Enhanced electrocatalytic degradation of bisphenol A by graphite/β-PbO2 anode in a three-dimensional electrochemical reactor. J. Environ. Chem. Eng. 9, 106072. https://doi.org/10.1016/j.jece.2021.106072.

Shokoohi, R., Gillani, R.A., Mahmoudi, M.M., Dargahi, A., 2018. Investigation of the efficiency of heterogeneous Fenton-like process using modified magnetic nanoparticles with sodium alginate in removing Bisphenol A from aquatic environments: kinetic studies. Desalination Water Treat. 101, 185–192. https://doi.org/10.5004/dwt.2018.21736.

Shuchi, S.B., Suhan, MdB.K., Humayun, S.B., Haque, M.E., Islam, MdS., 2021. Heat-activated potassium persulfate treatment of Sudan Black B dye: degradation kinetic and thermodynamic studies. Journal of Water Process Engineering 39, 101690. https://doi.org/10.1016/j.jwpe.2020.101690.

Simunovic, M., Kusic, H., Koprivanac, N., Bozic, A.L., 2011. Treatment of simulated industrial wastewater by photo-Fenton process: Part II. The development of mechanistic model. Chem. Eng. J. 173, 280–289. https://doi.org/10.1016/j.cej.2010.09.030.

Sonawane, S., Rayaroth, M.P., Landge, V.K., Fedorov, K., Boczkaj, G., 2022. Thermally activated persulfate-based Advanced Oxidation Processes — recent progress and challenges in mineralization of persistent organic chemicals: a review. Current Opinion in Chemical Engineering 37, 100839. https://doi.org/10.1016/j.coche.2022.100839.

Tsitonaki, A., Petri, B., Crimi, M., Mosbæk, H., Siegrist, R.L., Bjerg, P.L., 2010. In situ chemical oxidation of contaminated soil and groundwater using persulfate: a review. Crit. Rev. Environ. Sci. Technol. 40, 55–91. https://doi.org/10.1080/10643380802039303.

Wang, J., Wang, S., 2018. Activation of persulfate (PS) and peroxymonosulfate (PMS) and application for the degradation of emerging contaminants. Chem. Eng. J. 334, 1502–1517. https://doi.org/10.1016/j.cej.2017.11.059.

Wang, B., Wang, Y., 2022. A comprehensive review on persulfate activation treatment of wastewater. Sci. Total Environ. 831, 154906. https://doi.org/10.1016/j.scitotenv.2022.154906.

Yabalak, E., Ozay, Y., Vatanpour, V., Dizge, N., 2021. Membrane concentrate management for textile wastewater with thermally activated persulfate oxidation method. Water Environ. J. 35, 1281–1292. https://doi.org/10.1111/wej.12718.

Yan, B., Xu, D., Liu, Z., Tang, J., Huang, R., Zhang, M., Cui, F., Shi, W., Hu, C., 2021. Degradation of neurotoxin β-N-methylamino-L-alanine by UV254 activated persulfate: kinetic model and reaction pathways. Chem. Eng. J. 404, 127041. https://doi.org/10.1016/j.cej.2020.127041.

Yang, H., Graham, N.J.D., Wang, W., Liu, M., Yu, W., 2021. Evaluating and improving the reliability of the UV-persulfate method for the determination of TOC/DOC in surface waters. Water Res. 196, 116918. https://doi.org/10.1016/j.watres.2021.116918.

Zhang, Y., Chelme-Ayala, P., Klamerth, N., Gamal El-Din, M., 2017. Application of UV-irradiated Fe(III)-nitrilotriacetic acid (UV-Fe(III)NTA) and UV-NTA-Fenton systems to degrade model and natural occurring naphthenic acids. Chemosphere 179, 359–366. https://doi.org/10.1016/j.chemosphere.2017.03.112.